

Searching for Weather in Brown Dwarfs

C. G. Tinney^{1*} & A. J. Tolley^{1,2}

¹*Anglo-Australian Observatory, PO Box 296, Epping, N.S.W. 1710, Australia.*

²*Jesus College, Oxford University*

Accepted 13 November 1998. Received 7 November 1998; in original form 14 September 1998

ABSTRACT

We have used an innovative tuneable filter technique to carry out a search for the variability signatures of meteorological processes in the atmospheres of two nearby brown dwarfs. We find no evidence for variability in the L-type brown dwarf DENIS-P J1228-1547 in an observations spanning approximately half a rotation period (3 hours), and evidence for variability in the M-type brown dwarf LP 944-20 in multiple observations spanning approximately one third of a rotation period (1.5 hours).

Key words: methods: observational - techniques: spectroscopic - stars: atmospheres - stars: low-mass, brown dwarfs - stars: rotation - stars: spots

1 INTRODUCTION

The discovery of large numbers of brown dwarfs in recent years (q.v. Rebolo et al. 1998; Zapatero Osorio et al. 1999; Tinney 1998b) has meant that this field can finally move beyond the “Guinness Book of World Records” phase, and into a period where real understanding of brown dwarf properties is possible. Several major results have emerged from this increased understanding. The first of these is the fundamental importance of dust formation in the atmospheres of brown dwarfs (Allard et al. 1997; Tinney et al. 1998; Burrows & Sharp 1998). A few examples include: the dramatic change seen in the optical spectra of cool dwarf atmospheres as effective temperature (T_{eff}) drops below about 2000K (eg. Kirkpatrick et al. 1998), which is due to the depletion of plasma-phase TiO and VO as dust containing Ti and V condenses; and that clouds of yet another – presently unidentified – set of condensates lying above the photosphere, are thought to be responsible for the unusually steep optical spectrum of the brown dwarf Gl 229B (Schultz et al. 1998; Oppenheimer et al. 1998; Burrows & Sharp 1998).

A second fundamental property is that a large number of brown dwarfs are seen to be rapidly rotating (Martín et al. 1997; Tinney & Reid 1998), with rotational velocities of $v \sin i \approx 20 - 40$ km/s being common. At the typical radii of brown dwarfs ($0.1 R_{\odot}$, Burrows et al. 1989) this corresponds to rotation periods of 6-3 hours for brown dwarfs viewed equatorially. Similar rotation periods have been observed in a few of the very lowest mass stars (Martín et al. 1996). The combination of rapid rotation with cloud deck formation, logically leads to the prospect that rotationally driven me-

teorology may play as important a role in brown dwarfs, as it does in giant planets. Already observations suggest that circulation from lower to higher regions of the atmosphere of the Gl 229B may take place, resulting in the mixing of CO to the brown dwarf’s surface (Noll, Geballe & Marley 1997; Oppenheimer et al. 1998).

Since, however, we cannot obtain resolved images for brown dwarfs (as we can for the Solar system giant planets) detecting the signatures of meteorological effects must be made via time variability. Using Jupiter as a model, we would expect to observe variability; (1) on time scales similar to the rotation period of a brown dwarf (several hours), as storm features appear from beyond the limb, transit the disc, and vanish again; and, (2) on the timescales over which meteorological structures form and dissipate (weeks to months to centuries in the case of Jupiter). The detection of these effects will be complicated by the fact that low-mass stars are known to show variability due to the presence of spots and flares associated with stellar activity. Flares are observed as extremely high temperature events, producing significant ultra-violet radiation and strong line emission. The observations we describe below, are extremely insensitive to such effects. Star spots, however, are observed as regions of depressed effective temperature passing over the visible disc. This means they will have a similar timescale to the passing of meteorological features across the disc.

Most of the rapidly rotating cool dwarfs discovered to date show extremely small levels of chromospheric activity (Tinney & Reid 1998; Basri & Marcy 1995). It is therefore likely that magnetically induced spots will be weak, or absent in these objects. However, even if spots are present, they will not display the simple “dark patch” signatures seen in hotter stars, because their lower temperatures will significantly enhance dust condensation. Moreover, any spots that

* E-mail: cgt@aaoepp.aao.gov.au

are present will almost certainly interact with the “unspotted” level of cloud formation, and thereby contribute to the overall weather patterns in brown dwarfs. As our current understanding of both magnetically driven spot activity, and rotationally driven storm activity in brown dwarfs is meager indeed, observations of either or both are interesting – even if at present we cannot disentangle their effects.

We have carried out a first search for variability of a spectroscopic signature in brown dwarfs, which is sensitive to changes in T_{eff} and/or the extent of molecular depletion, by using a new charge-shuffling and frequency switching technique with the Anglo-Australian Observatory’s Taurus Tuneable Filter (TTF, Bland-Hawthorn & Jones 1998a,b). This technique extends that used by Deutsch, Margon & Bland-Hawthorn (1998) to study time variability at a single wavelength, by the use of multiple wavelengths. In particular, we have focussed on the two wavelength ranges shown in Fig. 1. The blue band (B1) lies on a strong TiO absorption feature in M-dwarfs at $\approx 2000\text{K}$. The strength of this band decreases with decreasing temperature as condensates containing Ti deplete the atmosphere of plasma-phase TiO. Measuring the colour difference between this band and a redder band (B2 in Fig. 1) as a function of time should therefore be sensitive to the passage of regions of different T_{eff} (and/or regions of increased or decreased dust condensation) across the visible disc of a brown dwarf.

2 OBSERVATIONS

Observations were carried out on the nights of 1998 February 25 and 26, and 1998 August 20 and 21 (UT), using the 3.9m Anglo-Australian Telescope with TTF and the MITLL2 $2\text{K}\times 4\text{K}$ $15\mu\text{m}$ pixel CCD. TTF comprises two high finesse, small spacing ($2=12\mu\text{m}$) etalons designed to deliver superior throughput, narrow-band imaging in the wavelength range $0.37\text{--}1.0\mu\text{m}$ (Bland-Hawthorn & Jones 1998a,b). Its operation has been integrated with the charge shuffling facilities of the AAO-1 CCD controllers to permit multiple exposures with rapid ($\sim 1\text{s}$) frequency switching. For these runs, the instrument was configured to operate through the TTF I₆ blocking filter ($\lambda=8380\text{--}8750\text{\AA}$) in two passbands centered near 8570\AA (B1) and 8725\AA (B2), with a full width at half-maximum (FWHM) spectral resolution of 30\AA . The exact central wavelengths measured on each of the two runs are given in Table 1. The observations carried out in 1998 February were thought to be photometric (though no flux standards were observed as our program is entirely differential), but those obtained in 1998 August were affected by cloud and fog, which severely limited the amount of data which could be obtained.

Figure 1 shows where the B1 and B2 band-passes fall in relation to the night-sky spectrum, and the spectra of a cool dwarf sequence. The wavelengths chosen avoid bright night-sky emission, with B1 lying at a wavelength showing strong TiO absorption in $T_{\text{eff}}\approx 2000\text{K}$ M-dwarf spectra, which is weak or absent in cooler spectra. The B2 band, on the other hand, lies in a wavelength range almost unaffected by changes in T_{eff} down to the coolest L-dwarf ($\approx 1600\text{K}$). At $\approx 1000\text{K}$ discrete molecular absorption seems to be totally absent in both bands, but it is likely that broad H₂O absorption is present (M.Marley, priv.comm.) in both, and

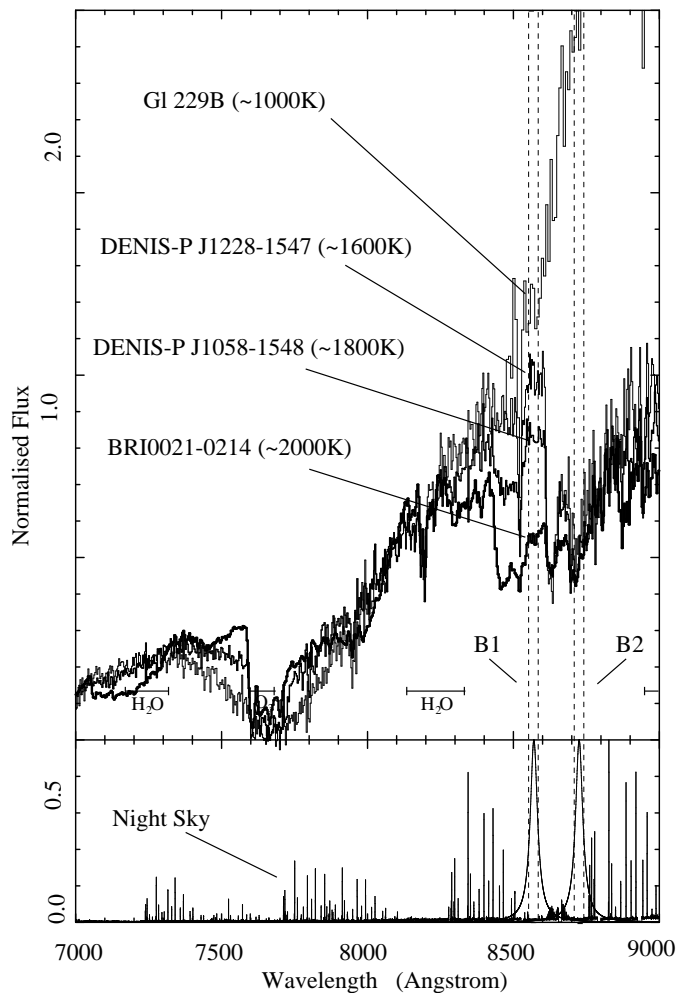


Figure 1. Location of the B1 and B2 bands used in our experiment. The lower panel shows the B1 and B2 band-passes adopted, superimposed on a night sky spectrum with the locations of terrestrial absorption marked. The upper panel highlights the variation in the B1-B2 colour as a function of T_{eff} , via a sequence of three cool dwarfs, which have been normalized to have the same flux in the I band. The spectra and approximate T_{eff} shown are due to Delfosse et al. 1997, Martín et al. 1997, Allard et al. 1996, Tinney et al. 1998 & Oppenheimer et al. 1998.

that the band fluxes are determined by a combination of small particle dust opacity (Burrows & Sharp 1998) and H₂O absorption.

Observations were performed through a specially constructed “slot” mask, which gave a $28''\times 6.2'$ (or 78×1000 pixel) field of view. Because this field is considerably smaller than our $2\text{K}\times 4\text{K}$ CCD, we are able to use charge shuffling to acquire up to 30 independent observations of the “slot” field before CCD readout is required. For these observations (cf. Fig. 2) a single exposure consists of a shuffle sequence as follows: (1) a 60s exposure in B1; (2) 1s of dead time while TTF is re-configured and charge is shuffled; (3) a 60s exposure in B2; and (4) another 1s of dead time. This sequence is repeated 15 times, after the detector is read out at a gain of $1.1\text{e}^-/\text{adu}$ and a read noise of 2e^- . Each 30 minute observation therefore produces a 1000×2740 pixel image, comprising

Table 1. Observing Log

Object	α, δ^a (J2000.0)		I^a	UT Date ^b	Exposure (s)	B1 ^c (Å)	B2 ^c (Å)	$\Delta\lambda^d$ (Å)
DENIS-P J1228-1547	12:28:13.8	-15:47:11	18.2	1998 Feb 25, 13:54:39.9	6×30×60	8570.6	8725.4	30
LP 944-20	03:39:34.6	-35:25:51	14.2	1998 Feb 26, 09:59:01.0	4×30×60	8570.6	8725.4	30
LP 944-20	03:39:34.6	-35:25:51	"	1998 Aug 20, 16:28:51.1	4×30×60	8571.0	8723.1	30
LP 944-20	03:39:34.6	-35:25:51	"	1998 Aug 21, 14:56:39.2	4×30×60	8571.0	8723.1	30

a – Positions and magnitudes due to Delfosse et al. 1997 and Tinney 1996. These references also contain finding charts.

b – This is the time at which the shutter was opened for the first exposure taken on this object on this date.

c – Central wavelengths for B1 and B2 were slightly different between February and August observing runs.

d – Bandwidth as FWHM, which are the same for both bands. The band-passes are extremely well approximated as Lorentzian.

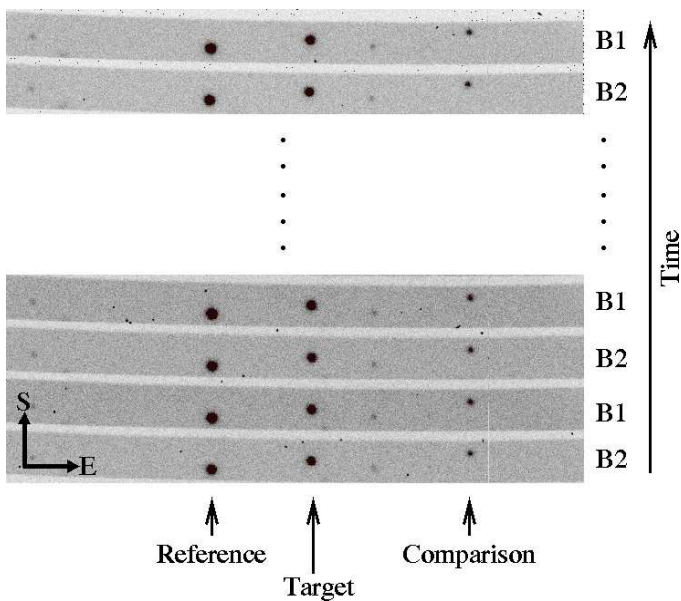


Figure 2. TTF shuffle data for LP 944-20 from 1998 August 21 (UT), showing the nature of the time series images acquired, and the reference, comparison and target stars used (cf. section 3.3). The curved field edges are due to the astrometric distortion present at the edge of the Taurus 2 field.

fifteen consecutive 60s observations in B1 interleaved with fifteen consecutive 60s observations in B2.

The objects observed are listed in Table 1. DENIS-P J1228-1547 is an L-type (Kirkpatrick et al. 1998) brown dwarf with mass less than $0.065 M_{\odot}$, and age less than 1 Gyr (Tinney, Delfosse & Forveille 1997; Martín et al. 1997). Martín et al. (1997) report a rotation velocity of $v \sin i \approx 20$ km/s for DENIS-P J1228-1547. LP 944-20 (also known as BRI 0337-3535) has a mass of $0.060 \pm 0.004 M_{\odot}$ and an age in the range 475-650 Myr (Tinney 1998a). Tinney & Reid (1998) report a rotation velocity of $v \sin i = 28 \pm 2$ km/s for LP 944-20.

3 ANALYSIS

3.1 Image processing

Each of the resulting images was bias subtracted using a 20 pixel overscan region. Domeflat observations were taken in exactly the same manner as target observations. In order to

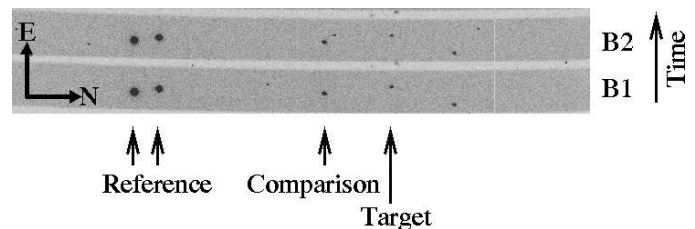


Figure 3. TTF shuffle data for DENIS-P J1228-1547 from 1998 February 25 (UT), showing the reference, comparison and target stars used (cf. section 3.3). Note that the order in which the B1 and B2 bands were observed is reversed from that used in the August run.

avoid fluctuations in the domeflat illumination during the course of a shuffle sequence, these domeflats were broken up into thirty 1000×90 pixel sub-segments. Each of the 15 “copies” of the B1 and B2 sub-segments were then averaged, and replicated back into a full 1000×2740 pixel image. The flattened data images displayed $\approx 5\%$ residual variations in sky background, indicating that in the future, more care will be required in obtaining flat-fields for this type of data. However, since this experiment aims to perform *differential* photometry, this is not considered a serious flaw of the current data set. In order to ensure that un-illuminated parts of the shuffle image are ignored in subsequent photometry, the flat fields were also used to construct a mask image, which flagged all un-illuminated pixels as bad.

3.2 Calibration

A CuAr arc spectrum, acquired by stepping through a large range in plate spacing, was used to derive wavelength calibrations, and to confirm the 30 \AA (FWHM) resolution. Observations were also made on February 25 of the standard star CD-32 9927 (Hamuy et al. 1994). From the published spectro-photometry for this star and the known central wavelengths and bandwidths, we estimated the relative fluxes of CD-32 9927 through our B1 and B2 bandpasses. The intrinsic ratio of the B1/B2 flux for CD-32 9927 is 1.00871, whereas we observe 1.1036 ± 0.0010 , which implies that the total throughput of the B1 passband is 9.4% higher than that of the B2 passband. This is almost exactly what would be expected from the throughput of the I_6 blocking filter at these wavelengths.

3.3 Photometry

Photometry was performed using the DAOPHOT package within the IRAF environment. Experiments were performed with both aperture and point-spread-function (PSF) photometry. Owing to the variation in seeing observed throughout a given 30 minute shuffle sequence, it was found that if PSF fitting was to be used, the PSF had to be evaluated independently for each 1000×90 pixel sub-segment. This usually resulted in the PSF being determined by just two stars. However, since our fields are uncrowded, the major reason for using PSF photometry is to make our photometry more robust against cosmic ray hits. In this case, the PSF is only being used as a weighting function, making the small number of stars used to determine it of minor significance.

The procedure used was as follows; (1) stars of interest were selected by hand from a single image; (2) the aperture photometry function of DAOPHOT was then used to centroid and photometer these stars in all images; (3) PSFs were calculated for each sub-segment and (4) PSF photometry was obtained using these PSFs. Comparison of PSF and aperture photometry showed them to produce essentially identical performance, with the exception that the PSF photometry proved more robust at rejecting contamination by cosmic rays. It is therefore this PSF data which we report here.

In order to correct the photometry of our target object for changes in atmospheric transparency, we adopted the brightest available stars in each field as zero-point *reference* objects. Figure 4a shows the values of these zero-points for two sample sequences of data – one taken in photometric conditions, and the other taken in non-photometric conditions. In order to test these zero-points, we further identified a *comparison* object in each field, which was not used in deriving the zero-point. The differential photometry for these *comparison* objects is shown in Fig. 4b for the data shown in Fig. 4a, confirming that indeed we do remove atmospheric effects. For DENIS-P J1228-1547 the *comparison* adopted is 1.3 magnitudes brighter than our target star, while for LP 944-20 it is 1.6 magnitudes fainter.

Lastly, Fig. 5 shows the differential photometry for our target objects. In each figure we also show the colour B1-B2, derived from each B1/B2 observation pair, as well as the data binned into 10 minute intervals (ie. 5 minutes of exposure time at a duty cycle of 50%). The uncertainties plotted are those produced by the DAOPHOT aperture photometry code (based on photon-counting) and have been appropriately propagated through all steps. We have plotted the three observations made of LP 944-20 separately in each case. Because these observations are so widely separated in time, we do not consider the differences in magnitude level *between* these observations anywhere near as significant as differences *within* a shuffle sequence.

3.4 Comparison Objects

In order to determine whether we have made a significant detection of variability, it is necessary to define our null hypothesis – ie. what does a non-detection look like. Kolmogorov-Smirnov (K-S) tests (eg. Press et al. 1986) were used to test the hypothesis (Hypothesis A) that the *comparison* objects' residual magnitude distributions were consistent with being

Table 2. Results of Statistical Tests

Object ^a	Hypothesis A ^b			Hypothesis B ^c		
	B1 (%)	B2 (%)	B1-B2 (%)	B1 (%)	B2 (%)	B1-B2 (%)
DENIS 1228	59.9	56.8	38.9	99.7	62.3	28.5
LP 944-20	88.9	13.7	60.3	15.3	2.0	20.4
LP 944-20	24.2	78.0	84.7	85.7	1.1	30.4
LP 944-20	94.2	68.9	92.3	2.2	97.6	38.5

a – the listed order is the same as used in Table 1.

b – see section 3.4. *c* – see section 3.5.

drawn from a sample with constant magnitude and scatter produced by the mean photon-counting uncertainty for that observing sequence. The results of these tests are shown in Table 2. We conclude from these that photon-counting is indeed a reasonable way of estimating the scatter produced about the mean magnitude of a non-varying object. This suggests both that our reference objects are not variable, and that atmospheric effects have been removed to a level where they are smaller than photon-counting uncertainties.

3.5 Target Objects

We can therefore use the photon-counting uncertainties for our target objects to define a null hypothesis for the detection of variability (ie magnitude constancy with scatter consistent with photon-counting uncertainties – Hypothesis B) for our target objects. The results of K-S tests for such a hypothesis are shown in Table 2.

4 DISCUSSION

Due to the shortness of the time series we were able to acquire, it is impossible to seek any periodicities in this data. We therefore limit ourselves to setting limits on the extent of variability in these brown dwarfs, and addressing the cloud implications of this variability.

4.1 DENIS-P J1228-1547

Figure 5 and Table 2 fairly convincingly demonstrate that we detect no evidence for variability in either the B1 or B2 magnitudes, or the B1-B2 colour, in DENIS-P J1228-1547. We therefore ask, what limits this places on the possible presence of regions of differential T_{eff} during our 3 hour observation? The data shown in Fig. 5 indicate we can rule out the presence of changes in B1-B2 of greater than 0.096 magnitude over ten minute periods (ie five 5 minute observations) at the $3\text{-}\sigma$ level. In order to estimate the T_{eff} change such a limit corresponds to, we have integrated the spectra shown in Fig. 1 over our B1 and B2 bandpasses, to obtain a calibration between B1-B2 colour and effective temperature, which we show in Fig. 6. We emphasise that we aim to use this calibration *only* to estimate temperature changes – it is *not* useful for estimating absolute effective temperatures. Unfortunately, no spectra are available in the $T_{\text{eff}}=1000\text{--}1600\text{K}$ range, though the available data suggest that somewhere in this range the B1-B2 colour “turns around” as the CrH and FeH bands in which the B2 band lies become weak

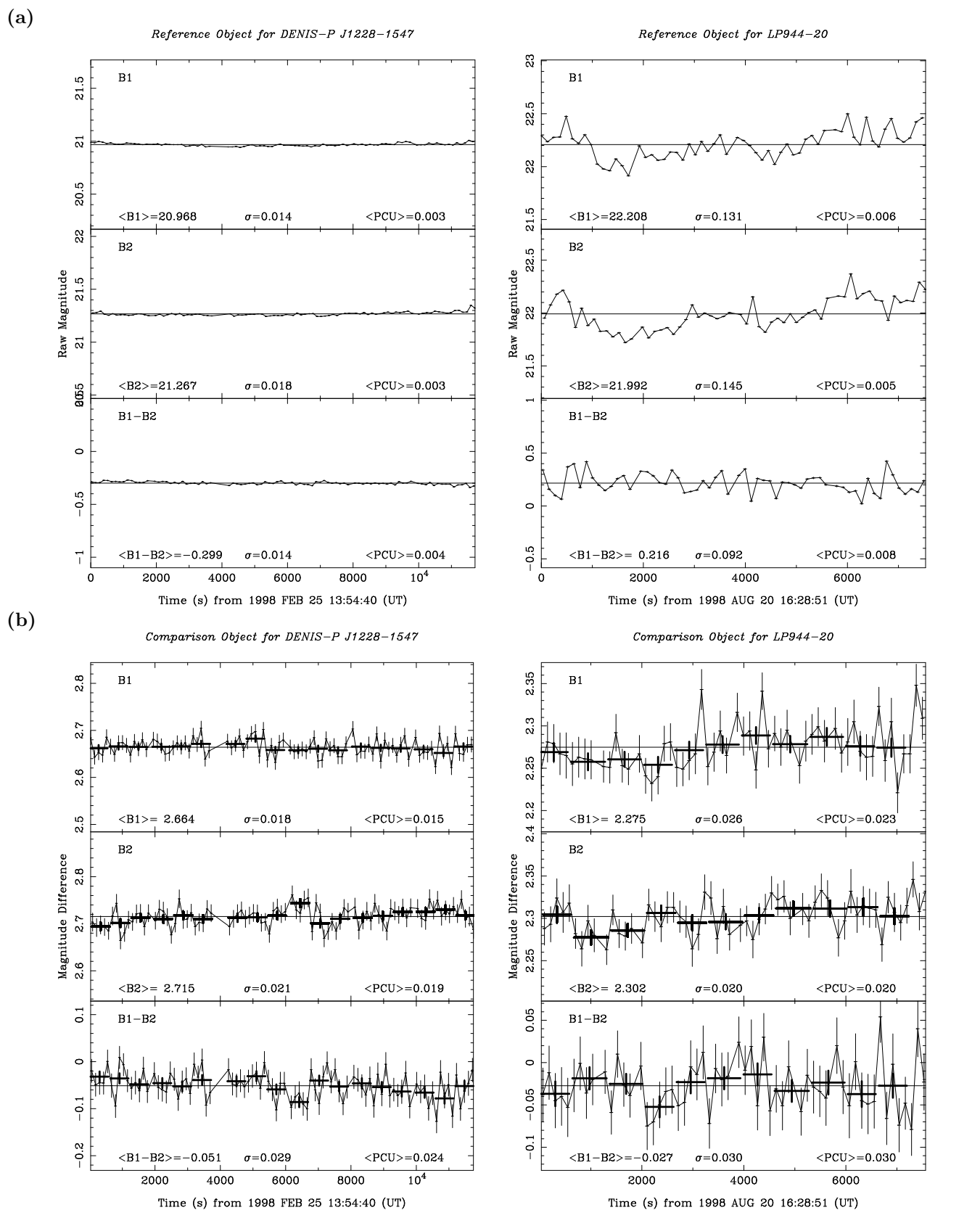


Figure 4. Sample time series data for (a) reference and (b) comparison stars. In each panel the weighted mean magnitude ($\langle B1 \rangle$, $\langle B2 \rangle$ and $\langle B1-B2 \rangle$), the standard deviation (σ) and the mean photon-counting uncertainty ($\langle PCU \rangle$) is shown. In the (b) panels we also show as heavy crosses, the data binned as ten minute averages (ie 5×1 minute exposures).

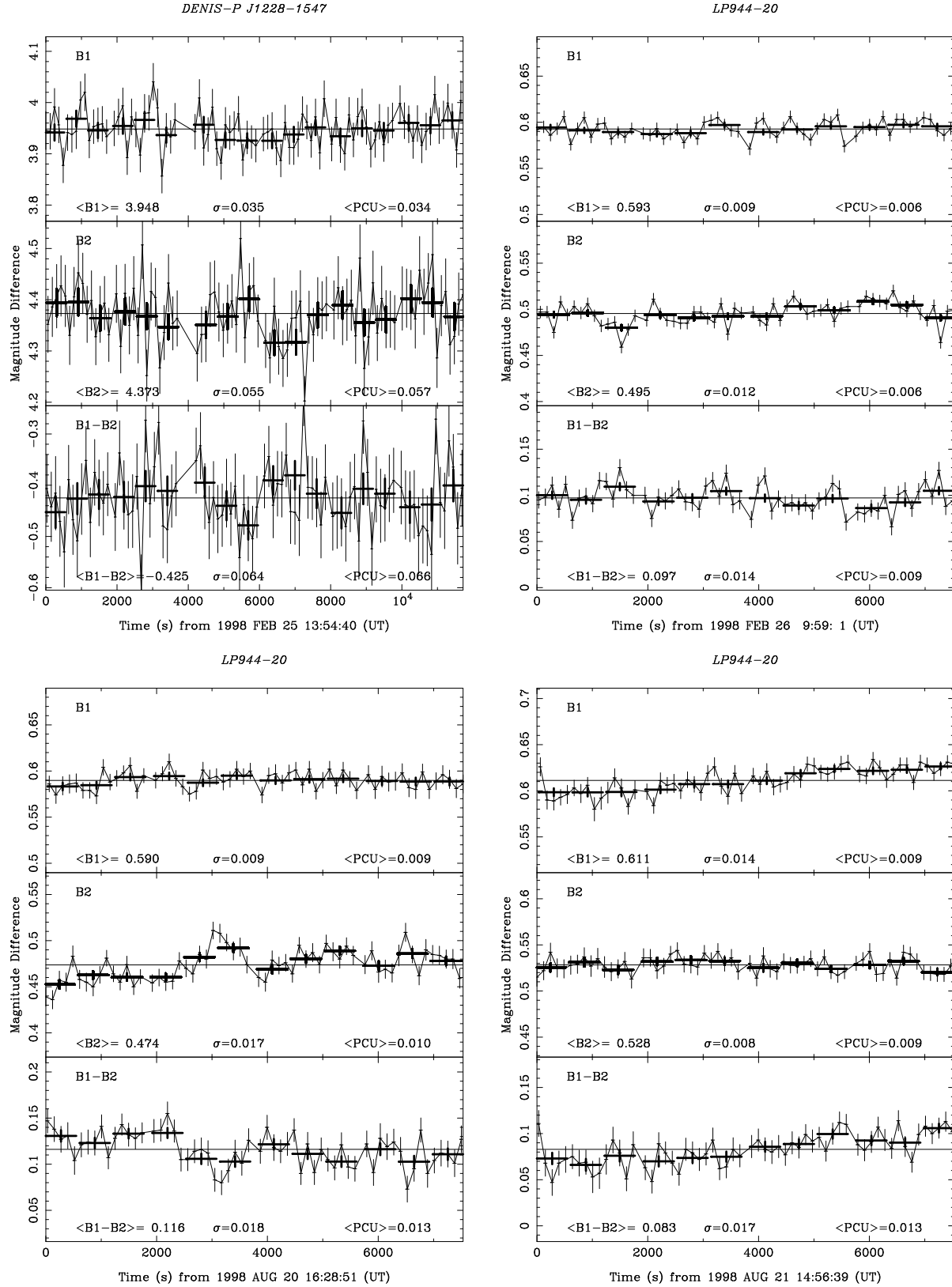


Figure 5. Time series data for the observations of the target objects listed in Table 1. In each panel the weighted mean magnitude ($\langle B1 \rangle$, $\langle B2 \rangle$ and $\langle B1-B2 \rangle$), the standard deviation (σ) and the mean photon-counting uncertainty ($\langle PCU \rangle$) is shown. We also show as heavy crosses, the data binned as ten minute averages (ie 5×1 minute exposures).

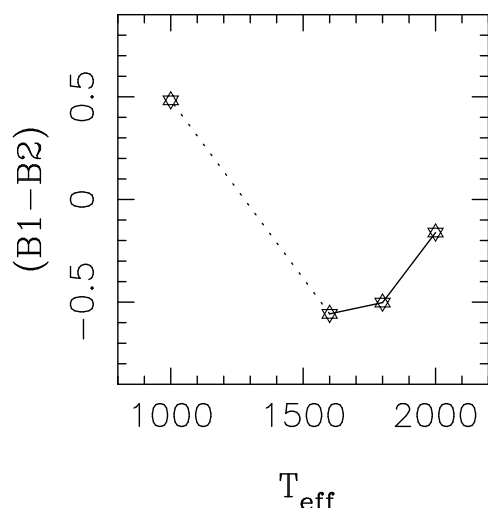


Figure 6. Calibration curve for differential temperatures as a function of changes in B1-B2 colours. B1-B2 estimated from spectra of Fig. 1 and T_{eff} estimates from the references in Fig. 1. Owing to the lack of data in the range $T_{\text{eff}}=1000\text{-}1600\text{K}$, this portion of the curve is drawn as dashed.

at very low temperatures (Kirkpatrick et al. 1998; Burrows & Sharp 1998). The data available, suggest that a B1-B2 colour change of 0.096 mag could correspond to a ΔT_{eff} of either +220K or -70K over the entire visible disc of the brown dwarf – with the change to lower temperature being particularly poorly constrained by the available data. More extreme changes over smaller regions of the visible disc are, of course, allowed by these limits.

These limits are not particularly tight, largely because of the weak limits we place on B1-B2 variation due to the faintness of DENIS-P J1228-1547. It is planned to acquire better data in the future over longer observing periods in order to improve these limits. There is also a systematic uncertainty present in the interpretation of these results due to the lack of objects with published spectra cooler than 1600K. This can be expected to change as new L-dwarfs are discovered by the 2MASS and DENIS surveys in the near future (Skrutskie et al. 1997; Epchtein et al. 1997).

4.2 LP 944-20

The fact that LP 944-20 is considerably brighter than DENIS-P J1228-1547 has allowed us to acquire much better data for it. The results of the K-S tests shown in Table 2 clearly show that in each of the data runs acquired at least one of the B1 or B2 time series is inconsistent at the 98% confidence level with the absence of variability. This can clearly be seen in Figure 5 in both the unbinned and binned data. In particular, we see a rising trend in the B2 data for August 20 and in the B1 data for August 21, and short period anomalies in the February 26 and August 20 B2 data. These effects tend to be washed out in the colour data by the scatter in the other passband, but remain visible.

A suspicion may remain that the variation we see is due to the single *reference* object adopted, rather than LP 944-20 itself. In Figure 7 we therefore show the B1 *comparison* object data for August 21, with the binned *target* object data overlaid. It can be clearly seen that the variation we

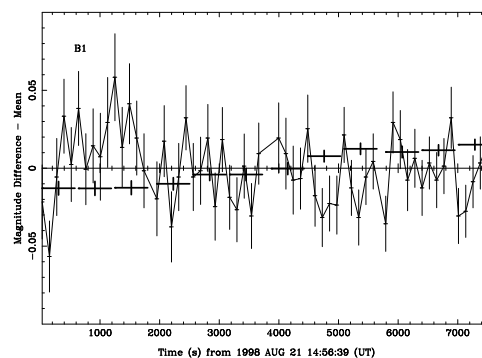


Figure 7. Comparison of a set of LP 944-20 binned *target* star and unbinned *comparison* star observations. This demonstrates that although the photon-counting uncertainties for the *comparison* star are larger than those LP 944-20, they do not hide the observed variation seen in LP 944-20 – the variation seen is therefore not due to the *reference* star adopted.

observe in LP 944-20 is not present in the *comparison* star, demonstrating that the variability we see *is* due to LP 944-20.

The data acquired on August 20 and 21 shows tantalising evidence for rotational modulation, with the B1-B2 colour falling for 2 hours on August 20, and rising on August 21. However, in light of the fact that we have only 2 hour chunks of data for an object expected to have a ≈ 4.5 hour period, we make no attempt to set limits on the period. The fact that variability is so easily detected, however, offers exciting prospects for period determination from future observations in better conditions and with longer observing runs.

We believe the data presented in Fig. 5 shows convincing evidence for variability in the B1-B2 colour of LP 944-20 at the 0.04 magnitude (98% confidence or $2.3\text{-}\sigma$) level. Using the calibration shown in Fig. 6, this corresponds to an equivalent ΔT_{eff} change of $\approx 20\text{K}$ over the entire visible disc of the brown dwarf, or $\Delta T_{\text{eff}} \approx 80\text{K}$ over 25% of the disc, or $\Delta T_{\text{eff}} \approx 400\text{K}$ over 5% of the disc.

The short timescale variation seen in B2 and B1-B2 on August 20 at $\approx 3000\text{s}$ is interesting. With an expected period of ~ 4.5 hours (if observed equatorially), the observation of a ~ 20 minute event would seem to imply either that the brown dwarf must have a period significantly shorter than 4.5 hours (and therefore a significant inclination angle) or that its photosphere contains a large number of clouds, and that we are observing the integrated effect of their appearance and disappearance beyond the brown dwarf’s limb. In either case, they offer an exciting prospect for longer observations and period determination.

It is also interesting that in LP 944-20, we see evidence for variability in *both* the B1 and B2 magnitudes. Examination of Fig. 1 might suggest that the passage of dust clouds across the disc would be most likely to be seen in the B1 passband alone, since it is here that the effect of TiO depletion is strongest. However, the exact height at which dust clouds would form in L-dwarfs is far from clear – the case of G1229B, at least, suggests that some dust clouds may also form above the photosphere (Burrows & Sharp 1998), which dim both B2 and B1, and cause a reddening of B1-B2. As, moreover, is the materials from which clouds would form –

clouds rich in Cr or Fe, would deplete CrH and FeH causing changes in B2 rather than B1). In other words, the simplest picture of cloud formation is probably an over-simplification. Further work on brown dwarf meteorology will be required before we can develop a detailed understanding.

5 CONCLUSIONS: THE FUTURE

We have carried out a first series of observations aimed at observing meteorological effects in brown dwarfs, using an innovative charge-shuffling and frequency-switching technique. We find no evidence for variability in our chosen spectroscopic signature in the brown dwarf DENIS-P J1228-1547, but some evidence for variability in the hotter brown dwarf LP 944-20. The most obvious future development required in the study of brown dwarf weather is to target a larger sample of objects with more extensive observations. Several technical advances also offer exciting prospects. At present we observe each passband in 60s interleaved exposures. In future, we will implement a more elegant charge-shuffling scheme to switch between bands on much shorter (~ 10 s) timescales, allowing us to obtain much longer observations in the B1-B2 colour, while retaining near-simultaneity, and therefore placing better limits on faint targets. TTF can also be operated at larger bandwidths than were adopted in this experiment, again improving signal-to-noise on faint targets. And lastly, we hope to implement frequency-switching in combination with continuous read-out of our CCDs, allowing us to obtain arbitrary length time-series, instead of being limited to the current 30 observations. This improvement will also allow us to use larger field masks, permitting a larger ensemble of reference stars. In summary, while the data obtained to date shows there is already reason to believe current techniques can make headway in the study of brown dwarf weather, future improvements can be expected to considerably expand our possibilities.

Acknowledgments

This paper is based on observations made at the Anglo-Australian Telescope, Siding Spring, Australia. The authors would like to thank M.Marley for helpful comments, E.Martín for a thorough referees report, the AAT staff for their thorough and professional assistance throughout this observing program, and to thank the TTF team for providing an instrument of outstanding power and versatility.

REFERENCES

- Allard F., Hauschildt P., Alexander D.R. & Starrfield S. 1997, *ARA&A* 35, 137
 Allard F., Hauschildt P., Baraffe, I. & Chabrier, G. 1996, *ApJ*, 465, L123
 Basri, G. & Marcy, G.W. 1995, *AJ*, 109, 762
 Bland-Hawthorn, J. & Jones, D.H. 1998a, *PASA*, 15, 44
 Bland-Hawthorn, J. & Jones, D.H. 1998b, in *Optical Astronomical Instrumentation*, SPIE, 334, 5, in press
 Burrows A., Hubbard W.B. & Lunine J.I. 1989, *ApJ* 345, 939
 Burrows, A. & Sharp, C.M. 1998, *ApJ*, submitted (astro-ph/9807055)

- Delfosse, X. et al. 1997, *A&A*, 327, L25
 Deutsch, E.W., Margon, B. & Bland-Hawthorn, J. 1998, *PASP*, 110, 912
 Epchtein N., 1997, in *The Impact of Large Scale Near-IR Sky Surveys*, p. 15, ed. Garzon, F., et al., Kluwer: Dordrecht
 Hamuy, M., Suntzeff, N.B., Heathcote, S.R., Walker, A.R., Gigoux, P. & Phillips, M. 1994, *PASP*, 106, 566
 Kirkpatrick J.D. et al. 1998, *ApJ*, submitted
 Martín, E.L., Basri, G., Delfosse, X. & Forveille, T. 1997, *A&A*, 327, L29
 Martín, E.L., Zapatero Osorio, M.R. & Rebolo, R. 1996, in "Cool Stars, Stellar Systems and the Sun, 9th Cambridge Workshop", eds Pallavicini, R. & Dupree, A.K., *ASP Conf. Ser.* 109, 615
 Noll, K.S., Geballe, T. R. & Marley, M. S. 1997, *ApJ*, 489, L87
 Oppenheimer B.R., Kulkarni S.R., Matthews K. & van Kerkwijk, M.H. 1998, *ApJ* 502, 932
 Press, W.H., Flannery, B.P., Teukolsky, S.A. & Vetterling, W.T. 1986, *Numerical Recipes*, p472, Cambridge University Press: Cambridge
 Rebolo, R., Martín, E.L. & Zapatero Osorio, M.R. (eds) 1998, *Brown Dwarfs and Extrasolar Planets*, *ASP Conf.Series.* 134
 Schultz A.B. et al. 1998, *ApJ* 492, L181
 Skrutskie. M.F., 1997, in *The Impact of Large Scale Near-IR Sky Surveys*, p. 25, ed. Garzon, F., et al., Kluwer: Dordrecht
 Tinney, C.G. 1996, *MNRAS*, 281, 644
 Tinney, C.G. 1998a, *MNRAS*, 296, L42
 Tinney, C.G. 1998b, *Nature*, in press
 Tinney, C.G., Delfosse, X. & Forveille, T. 1997, *ApJ*, 490, L95
 Tinney, C.G., Delfosse, X. Forveille, T. & Allard, F. 1998, *A&A*, 338, in press
 Tinney, C.G. & Reid, I.N. 1998, *MNRAS*, in press
 Rebolo, R. & Zapatero Osorio, M.R. (eds) 1999, *Very Low-mass Stars and Brown Dwarfs in Stellar Clusters and Associations*, Cambridge University Press: Cambridge, in preparation